Heliyon 10 (2024) e38746

Contents lists available at ScienceDirect

Heliyon

journal homepage: www.cell.com/heliyon

Research article

Exploring the impact of Joule heating and Brownian motion on assisting and opposing flows in Eyring-Prandtl fluid

E.N. Maraj [a], Harsa Afaq [b,*], Ehtsham Azhar [b], Muhammad Jamal [b,c], Haitham A. Mahmoud [d]

[a] Department of Mathematics, National Skills University Islamabad, Pakistan
[b] Department of Mathematics, PMAS Arid Agriculture University Rawalpindi, Pakistan
[c] Department of Mathematics, Uppsala University, Uppsala, Sweden
[d] Industrial Engineering Department, College of Engineering, King Saud University, Riyadh 11421, Saudi Arabia

ARTICLE INFO

Keywords:
Thermophoretic effects
Brownian motion
Joule heating
Nonlinear system
Buoyancy region

ABSTRACT

Motivation and Objectives: The basic aim of this investigation is to explore the energy transfer impact on Eyring-Prandtl fluid, a topic that has not been previously examined, thereby paving the way for future researchers. The present literature is crucial for advancing thermal management in engineering applications. This study aims to numerically investigate the thermophoretic effects and Brownian motion of non-Newtonian nanofluid relying on Eyring-Prandtl fluid model across the stretching sheet. The sheet is along the vertical direction under applied magnetic field. Energy and mass transfer rate is explored by considering Joule heating, thermal radiations and chemical reaction effects.

Significance: The increasing potential of Eyring-Prandtl fluid lies in its applications in heat and mass transfer. The current analysis holds significant promise, particularly in scenarios where non-Newtonian working fluids are utilized. This research aids in optimizing industrial processes, designing of efficient cooling systems in electronic devices, and in polymer and food processing.

Methodology: The similarity transformations are utilized to turn a set of partial differential equations (PDEs) into a system of ordinary differential equation (ODE). The resulting system is modified and effectively solved by mean of numerical method known as the Runge Kutta method with bvp4c in MATLAB.

Outcomes: Graphical results show the behavior of several physical parameters across boundary layers of buoyancy assisting and buoyancy opposing region. The magnetic field enhances the thermal conductance of the fluid flow that give rise to flow rate at the surface as well as within the boundary layers. The existing outcomes in the study are attained as a special case of current study. Eyring-Prandtl fluids, with their unique rheological properties can improve the design and efficiency of microfluidic systems used in various applications such as chemical synthesis, drug delivery, and biomedical diagnostics.

* Corresponding author.
E-mail address: harsaafaq357@gmail.com (H. Afaq).

https://doi.org/10.1016/j.heliyon.2024.e38746
Received 16 February 2024; Received in revised form 27 September 2024; Accepted 29 September 2024

Available online 2 October 2024

Nomenclature

u, v	Components of velocity ..... $m\,s^{-1}$	D_T	Thermophoresis Diffusion coefficient
u_w	Linear stretching velocity ..... $m\,s^{-1}$	D_B	Brownian motion coefficient
u_∞	Ambient velocity ..... $m\,s^{-1}$	ψ	Stream function
a, c, m_1, m_2	Constants	γ	Prandtl fluid
ν	Kinematic viscosity ..... $m^2\,s^{-1}$	δ	Elasticity
g	Gravitational acceleration ..... $m\,s^{-2}$	r	Stagnation symbol
β_T	Thermal expansion coefficient ..... K^{-1}	R	Buoyancy effects
β_C	Coefficient of volumetric expansion ..... K^{-1}	Pr	Prandtl parameter
σ	Electrical conductivity ..... S/m	Re	Reynolds number
ρ	Density ..... $kg\,m^{-3}$	Rd	Thermal radiation
B_o	Magnetic field intensity	Ec	Eckert number
k	Thermal conductivity ..... $Wm^{-1}\,K^{-1}$	S	Suction parameter
c_p	Heat Capacity ..... $J\,K^{-1}$	τ_w	Shear Stress
T	Fluid temperature ..... K	Cf_x	Skin friction coefficient
T_∞	Ambient temperature ..... K	Nu_x	Nusselt number
C	Concentration of nanoparticle ..... $mol\,m^{-3}$	Sh_x	Sherwood number

1. Introduction

Heat transfer phenomenon has been extensively studied in literature over the years. The problem of efficient removal and addition of heat to a system has been burning topic for scientist and engineers who have worked tirelessly to find feasible and cost effective solutions. Choi and Eastman [1] in Argonne laboratory managed to successfully modify convectional fluid used in heat transfer processes by addition of nanoscale metal material- so called nanofluids. The achievement proved to be groundbreaking as numerous researches have been carried out on the experimental as well as numerical front to further better the performance of nanofluids. Shorbagya et al. [2] numerically handled a problem of mixed convective nanofluid flow in trapezoidal channel in a porous medium. It was analyzed that the porous medium has a significant impact on the conduction mechanism in the channel. Peng et al. [3] used artificial neural networks to study the effects on a precipitated surface while conducting both experimental and numerical studies on heat transmission in Fe_3O_4/water nanofluid. It was determined that the introduction of thermal resistance results in a decrease in the boiling heat transfer coefficient on the copper surface. Using the Lattice Boltzmann approach, Chen et al. [4] examined the simulated convective flow of a nanofluid within a square assembly naturally. Their findings revealed that the velocity of the nanoparticles is significantly lower unlike to the base fluid, and a opposite effect of the electric field was observed in the interaction between the fluid and nanoparticles. Rehman et al. [5] investigated the impact of Cattaneo-Christov energy flux on the Darcy-Forchheimer medium flow of Sutterby nanofluid over a stretching plane, considering chemical reactivity and thermal radiation effects. The Soret and Dufour effects in a magnetohydrodynamic mixed convection flow of a Cross fluid produced by a moveable thin needle which were studied by Rehman et al. [6].

Further investigations can be seen in [7–17].

Non-Newtonian fluids have gotten enormous significance in recent years due to vast applications in the field of engineering and science. Applications of such fluids can be found in food processes, polymer manufacturing, oil reservoir engineering. Unlike the Newtonian fluids, no single relation can classify all kind of non-Newtonian fluids. Depending upon the shear stress tensor, these fluids have been classified. One such class exists in which the fluid exhibits viscoelastic behavior of which Prandlt fluid is an example. Eyring-Prandlt fluid model due to its unique explanation of viscoelastic behavior has been vigorous used in researches recently. Eid et al. [18] explored the homogeneous-heterogeneous chemical reaction in an electrically conducting environment setting Prandtl fluid to motion over a flate surface horizontally laid with the medium being porous in nature. They solved the model using R-K method and observed the positive impact of suction and thermal radiation on the heat transport rate. In another study, Patil et al. [19] scrutinized the flow of the chemically reactive and thermally radiating Prandtl nanoliquid over a stretching surface with thermophoretic and Brownian motion of nanoparticles. Their observations included that escalative radiation and Biot parameters tend to increase the temperature of the fluid. Bio-micronanofluidic channel flow of Prandtl fluid due the peristatsis and external applied magnetic field was inspected by Abbasi et al. [20]. It is observed that isothermal lines increased with surge in thermophoretic parameter. Shamshuddin et al. [21] examined the impact of changing chemical reactions and Ohmic heating on a non-Newtonian Prandtl hybrid nanofluid including water-based nanofluids to an extension of the leading edge. Patil et al. [22] used the Prandtl fluid model to investigate the magnetohydrodynamics of reactive hybrid nanofluid flow. The author direct interested readers to go through [23–29] for further insights on Prandtl fluid model. Li et al. [30] analyzed nonlinear radiative heat energy on a Buongiorno modeled micro liquid contained by an inclined porous plate, this work looks at the use of a unique numerical methodology called the shotting method. Mustafa et al. [31] examined the unsteady flow of a Newtonian fluid over a stretched sheet situated within a saturated porous medium, focusing on the thermal energy distribution around the stagnation point region. Cite [32,33].

Since its initiation, magnetohydrodynamics (MHD) has found itself at the helm of many applications pertaining to heat transport in fluids such as fusion reactors, MHD drug carriers, MHD pumps, biomedical engineering and in blood flow problems. The mathematical

formulation of MHD is carried out using Maxwell equations of electromegnatism and with special restrains imposed reduces to a body force influencing the fluid flow. Biswal et al. [34] established the least square method solution of a mathematical problem in the MHD nanofluid flow in a semi-porous channel with silver and copper nanoparticles. Govindasamy and Bangalore [35] analyzed the rate of heat and mass transmission through the Casson nanofluid thin liquid layer as it passes by a stretching sheet. Gomathy and Rushi Kumar [36] examined the intricate dynamics of heat transfer and thin-film flow in porous media, paying particular attention to how Al_2O_3 nanoparticles behave in relation to their form. Gomathy and Kumar [37] analyzed the energy transfer and erratic thin-film flow of a $Ag - H_2O$ nanofluid on a stretched sheet inserted into a porous medium. The efficiency of the method was checked by plotting the residual errors graphically. It has been noted that the application of an external magnetic field has a significant impact on the flow and energy transfer characteristics of nanofluids. In a study by Sabu et al. [38], it was discovered that in MHD convective ferrofluid flow, the Hall and Soret numbers have a detrimental effect on mass and heat transmission. In a similar way, Jawad et al. [39] observed that when the magnetic field intensity grew, the Nusselt number and velocity profile near the wall decreased. For further details on the effects of MHD, refer to... [40–50].

Industrial heat exchangers provide a noteworthy application for which studying aiding and opposing flow across a vertical surface is relevant. The dynamics of fluid flow are crucial in determining the heat transfer efficiency of heat exchanger design. Through thorough analysis of the behavior of both opposing and aiding flows, engineers can modify heat exchanger topologies in order to improve thermal performance. For example, assisting flows can promote convective heat transfer, increasing the effectiveness of heat exchange procedures. On the other hand, opposing flows can be deliberately used to control temperature differences and guarantee even heat distribution inside the heat exchanger. Two-dimensional incompressible non-Newtonian fluid (Williamson model) flow through a unique kind of curvilinear coordinate system was examined by Gadelhak et al. [51]. Zaheer et al. [52] developed an innovative mathematical framework for electro-osmotic boundary layer flow. Mekheimer and Ramadan [53] examined how radiation, magnetic fields, and chemical reactions affected a non-Newtonian Prandtl fluid containing nanoparticles and gyrotactic bacteria. Thus, comprehending and influencing these flow phenomena over vertical surfaces can have a substantial impact on the operation and design of heat exchangers in a variety of industries, which will ultimately lead to improved thermal management system cost- and energy-effectiveness.

Novelty: According to the writer's knowledge, no prior literature has addressed the problem of flow over a stretching sheet using the Runge-Kutta forth order technique. This study is also unique in that the impact of thermophoresis and brownian motion on the flow stability is thoroughly discussed. An intriguing study is conducted, and the findings are novel to the best of our expertise.

In assessing this inquiry, the present study provides answers to the following research queries:

- What are the implications of varying magnetic field strengths on fluid flow patterns?
- What insights can be gained from analyzing the interaction between Joule heating, Brownian motion?
- What novel phenomena emerge when analyzing the assisting and opposing flow of Eyring-Prandtl fluid?
- What avenues for further research are suggested and how can they contribute to advancements in fluid dynamics?

2. Problem definition and mathematical framework

Assume the stagnation point of mixed convection in two dimensions. A vertical Eyring-Prandtl nanofluid flow is seen along the porous sheet. It is considered that the fluid is contained inside the Cartesian plane when $x > 0$ and is steady and incompressible. Taking along the positive y-axis, the vertical stretching surface is extended in both directions with a linear stretching velocity $u_w(x) = ax$, for arbitrary constant a, keeping the origin at the previous location. The surroundings fluid speed with respect to time is expressed as $u_\infty(x) = cx$, where c is any random constant. Additionally, the definition of the stress tensor τ for the current fluid is [54]:

$$\tau = \frac{m_1 sin^{-1}\left[\frac{1}{m_2}\sqrt{(\frac{\partial u}{\partial y})^2 + (\frac{\partial v}{\partial x})^2}\right]}{\sqrt{(\frac{\partial u}{\partial y})^2 + (\frac{\partial v}{\partial x})^2}}\frac{\partial u}{\partial y}. \tag{1}$$

Here, m_1 and m_2 represent material constants.

There are two distinct configurations of fluid flow in relation to an external force or boundary condition: opposing and assisting flows. Here is a quick rundown of these ideas, including how to apply them to the mathematical formulation and what their physical equivalents entail:

When a fluid flow is assisting flow, its direction matches the direction of an outside force or boundary condition. This shows that the external force increases the flow velocity, increasing the flow rate or velocity in the force's direction. To account for the impact of the external force, assisting flow can be represented mathematically by including a positive component in the governing equations.

When there is opposing flow, the direction of the fluid flow goes against the direction of the boundary condition or outside force. This indicates that the external force is obstructing the flow velocity, which results in a drop-in flow rate or velocity in the force's opposite direction. The counteracting effect of the external force can be represented by a negative term added to the governing equations, which will incorporate opposing flow. Opposing flow in the context of the Navier-Stokes equations could be represented by an additional element in the momentum equation that opposes the external force.

Fig. 1 shows the pictorial presentation of the physical problem.

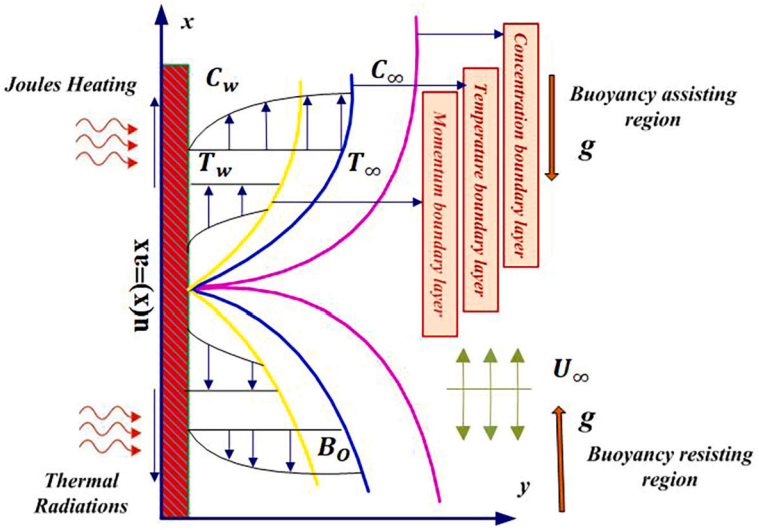

Fig. 1. Pictorial representation of flow.

2.1. Assumptions and constraints

- The flow is subjected to a constant magnetic field in a horizontal direction.
- An analysis has been conducted of the boundary-layer flow close to the sheet.
- The fluid being studied is Eyring-Prandtl nanofluid.
- The effects of thermophoresis and Joule heating are considered.

The constant horizontal magnetic field alters the fluid flow through magnetohydrodynamic effects and Lorentz forces induced by the magnetic field interact with the fluid. Boundary-layer flow near the sheet provides insights into how viscosity and shear stress affect the fluid's behavior close to the surface. Eyring-Prandtl nanofluid accounts for its non-Newtonian behavior and the presence of nanoparticles, which affect its rheological properties. Accounting for Joule heating and thermophoresis introduces additional heat sources and particle migration effects, respectively. Joule heating is commonly used in electric heaters, stoves, and other heating appliances. When an electric current flows through a conductor like a resistor, it produces heat as a result of the material's resistance. Additionally, Brownian motion affects the behavior of nanoparticles, playing a crucial role in several applications, including drug delivery systems and nanofluidics. Thermophoresis has applications in biology, where it can be used to manipulate biomolecules or cells in microfluidic systems for various purposes, including separation, sorting, and analysis.

2.2. Mathematical modeling

Based on the previously stated assumptions and taking into account boundary layer approximations, the set of governing PDE's may be expressed as follows, see [54].

$$\frac{\partial u}{\partial x} + \frac{\partial v}{\partial y} = 0\,, \tag{2}$$

$$u\frac{\partial u}{\partial x} + v\frac{\partial u}{\partial y} = u_\infty \frac{du_\infty}{dx} + \frac{\nu m_1}{2m_2^3}\left(2m_2^2 + (\frac{\partial u}{\partial y})^2\right)\frac{\partial^2 u}{\partial y^2} \pm g\,(\beta_T(T-T_\infty) + \beta_C(C-C_\infty)) - \frac{\sigma B_o^2}{\rho}(u-u_\infty), \tag{3}$$

$$u\frac{\partial T}{\partial x} + v\frac{\partial T}{\partial y} = \frac{k}{(\rho c_p)_f}\frac{\partial^2 T}{\partial y^2} + \frac{(\rho c_p)_p}{(\rho c_p)_f T_\infty}\frac{\partial T}{\partial y}\left(D_B T_\infty \frac{\partial C}{\partial y} + D_T \frac{\partial T}{\partial y}\right) + \frac{\sigma B_o^2}{(\rho c_p)_f}u^2 - \frac{1}{(\rho c_p)_f}\frac{\partial q}{\partial y}, \tag{4}$$

$$u\frac{\partial C}{\partial x} + v\frac{\partial C}{\partial y} = D_B\frac{\partial^2 C}{\partial y^2} + \frac{D_T}{T_\infty}\frac{\partial^2 T}{\partial y^2} - k_c(C-C_\infty). \tag{5}$$

From [55], using Rosseland approximation:

$$\frac{\partial q}{\partial y} = -\frac{16\sigma^* T_\infty^3}{3k^*}\frac{\partial^2 T}{\partial y^2}, \tag{6}$$

Here, κ^* represents the mean absorption coefficient, while σ^* denotes the Stefan-Boltzmann constant. Eq. (4) is transformed into (7) using Eq. (6). So Eq. (4) takes the form:

$$u\frac{\partial T}{\partial x}+\upsilon\frac{\partial T}{\partial y}=\frac{k}{(\rho c_p)_f}\frac{\partial^2 T}{\partial y^2}+\frac{(\rho c_p)_p}{(\rho c_p)_f T_\infty}\frac{\partial T}{\partial y}\left(D_B T_\infty\frac{\partial C}{\partial y}+D_T\frac{\partial T}{\partial y}\right)+\frac{\sigma B_o^2}{(\rho c_p)_f}u^2 + \frac{1}{(\rho c_p)_f}\frac{16\sigma^* T_\infty^3}{3k^*}\frac{\partial^2 T}{\partial y^2}. \tag{7}$$

In the equations above, the following variables are defined:

The velocities along the x- and y-axes are denoted by u and υ, respectively. The material constants are m_1 and m_2. The fluid's kinematic viscosity is indicated by ν. Indicating the electrical conductivity is σ. The base fluid's density is represented by ρ. The symbol for acceleration due to gravity is g. The thermal expansion coefficient is β_T. The coefficient of volumetric expansion of nanoparticles is β_C. The fluid's temperature and the ambient temperature are indicated by T and T_∞, respectively. The concentrations of nanoparticles inside and outside the boundary layer are denoted by C and C_∞, respectively. The heat conductivity is k. Here, c_p denotes the heat capacity.

D_T is the thermophoretic diffusion quantity, while D_B is the coefficient of Brownian diffusion. The corresponding boundary conditions are [54]:

$$\begin{aligned}&\text{for}\quad y=0,\quad u=u_w=ax,\quad \upsilon=\upsilon_w,\quad T=T_w,\quad C=C_w\\&\text{as}\quad y\to\infty,\quad u\to u_\infty,\qquad T\to T_\infty,\qquad C\to C_\infty.\end{aligned} \tag{8}$$

The temperature of fluid and nanoparticle concentration over the stretched surface are shown by T_w and C_w, respectively, while the fluid velocity over the permeable surface is indicated by υ_w. To transform the governing Eqs. (2), (3), (5), and (7) into non-dimensional form, consider the following similarity transformation [54].

$$\eta=y\sqrt{\frac{a}{\nu}},\quad f(\eta)=\frac{\psi}{x\sqrt{a\nu}},\quad \theta(\eta)=\left[\frac{T-T_\infty}{T_w-T_\infty}\right],\quad \phi(\eta)=\left[\frac{C-C_\infty}{C_w-C_\infty}\right], \tag{9}$$

where the ψ is stream function. The stream function is used to specify the components of velocity as $u=\frac{\partial\psi}{\partial y}$ and $\upsilon=-\frac{\partial\psi}{\partial x}$. Utilizing variables in Eq. (9), the governing Eqs. (2), (3), (5) and (7) along with boundary conditions in Eq. (8) in a non-dimensional form is given as:

$$\gamma f'''-(f')^2+ff''+\delta(f'')^2f'''+M\,(r-f')+r^2+\epsilon\,(\theta+R\phi)=0, \tag{10}$$

$$\left(1+\frac{4}{3}Rd\right)\theta''+Prf\theta'+PrNb\theta'\phi'+PrNt(\theta')^2+MPrEc(f')^2=0, \tag{11}$$

$$\phi''+LePrf\phi'+\frac{Nt}{Nb}\theta''-LePr\beta\phi=0. \tag{12}$$

The relevant boundary conditions after using transformations are

$$\left.\begin{aligned}&f\,(0)=S,\quad f'\,(0)=1,\quad \theta\,(0)=1,\quad \phi\,(0)=1\\&f'\to r,\quad \theta\to 0,\quad \phi\to 0\quad\text{for}\quad \eta\to\infty.\end{aligned}\right\} \tag{13}$$

Where prime denotes the distinction with regard to η. The equations presented above incorporate a diverse array of parameters that characterize various physical phenomena. These include:

Fluid Parameter of Eyring-Prandtl γ, Leverage δ, Parameter of Stagnation r, Magnetic Field Strength M, Buoyancy temperature parameter ϵ, Buoyancy concentration parameter ϵ^*, Ratio of buoyancy R, Grashof Thermal Number Gr_t, Number of Solutal Grashof Gr_c, Number of Prandtl Pr, The Reynolds Number, or Re_x, Quantity of Brownian Motion Nb, Lewis Number Le, Parameter for thermophoresis Nt, Thermal Radiation coefficient Rd, The Eckert Number Ec, and Chemical reaction parameter β Suction/Injection Parameter S.

Each of these parameters plays a crucial role in understanding the intricate behaviors of fluid dynamics and thermal processes described within the equations. The expressions for the aforementioned parameters are as follows Eq. (14):

$$\left.\begin{aligned}&\gamma=\frac{m_1}{m_2},\quad \delta=\frac{a^3x^2m_1}{2m_2^3\nu},\quad r=\frac{c}{a},\quad \epsilon=\frac{Gr_t}{(Re_x)^2},\quad \epsilon^*=\frac{Gr_c}{(Re_x)^2},R=\frac{\epsilon^*}{\epsilon},\\&\left[Gr_t=\frac{g\beta_T(T_w-T_\infty)x^3}{\nu^2}\right],\quad Gr_c=\left[\frac{g\beta_C(C_w-C_\infty)x^3}{\nu^2}\right],\quad Re_x=\frac{u_wx}{\nu},\\&Pr=\frac{\nu}{\alpha},\quad Nb=\frac{(\rho c_p)_pD_B(C_w-C_\infty)}{\nu(\rho c_p)_f},\quad Nt=\frac{(\rho c_p)_pD_T(T_w-T_\infty)}{\nu(\rho c_p)_f},\\&Le=\frac{\alpha}{D_B},\quad Ec=\frac{u_w^2}{c_p(T_w-T_\infty)},\quad Rd=\frac{4\sigma^*T_\infty^3}{3k^*k},\quad \beta=\frac{k_c}{a},\quad S=-\frac{\upsilon_w}{\sqrt{c}\nu}\end{aligned}\right\} \tag{14}$$

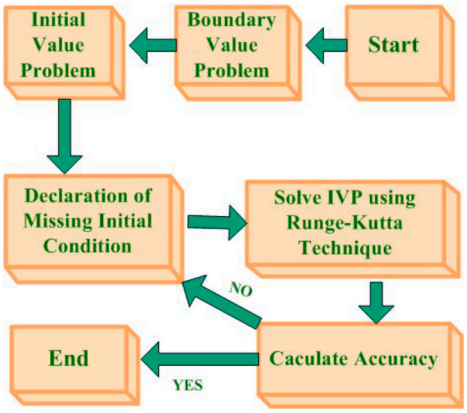

Fig. 2. Flow chart of numerical scheme.

Note that $S<0$ indicates injection and $S>0$ indicates suction. In Eq. (3), the sign $\pm$ denotes the combined effect of assisting and opposing flow of buoyancy force for $R>0$. The drag force at the surface, along with the energy and mass transfer rates, is determined using the Sherwood number Sh_x, the Nusselt number Nu_x, and the skin friction coefficient C_{f_x}, which are defined as follows:

$$Cf_x=\left[\frac{\tau_w}{\rho u_w^2}\right],\quad Nu_x=\left[\frac{xq_w}{k(T_w-T_\infty)}\right],\quad Sh_x=\left[\frac{xq_m}{D_B(C_w-C_\infty)}\right], \tag{15}$$

where the shear stress, heat, and mass fluxes are denoted by τ_w, q_m, and q_w, respectively, and are defined as;

$$\tau_w=\mu\left(\frac{m_1}{m_2}\frac{\partial u}{\partial y}+\frac{m_1}{(6m_2)^3}\left(\frac{\partial u}{\partial y}\right)^3\right),\quad q_w=-k\left(\frac{\partial T}{\partial y}\right)_{y=0},\quad q_m=-D_B\left(\frac{\partial T}{\partial y}\right)_{y=0}. \tag{16}$$

Sherwood numbers, Nusselt numbers, and dimensionless coefficients of skin friction are symbolized as

$$\begin{aligned}&(Re_x)^{1/2}\,Cf_x=\gamma\,f''(0)+\delta\,(f''(0))^3,\quad (Re_x)^{-1/2}\,Nu_x=-\theta'(0),\\&(Re_x)^{-1/2}\,Sh_x=-\phi'(0).\end{aligned} \tag{17}$$

Where, Eq. (15) and Eq. (16) is dimensional form of physical quantities. While Eq. (17) is non-dimensional form which is used to obtain the tabulated values.

3. Procedure of solution

The shooting method is used in conjunction with the Runge Kutta fourth order methodology to get a numerical solution for non-linear ordinary differential equations. This approach is frequently used in the literature since it is dependable and simple to utilize. The higher order ODE's Eqs. (10) - (13) are transformed into the first order ODE's using successive substitutions Eq. (18). The specifics are condensed and made clearer for readability, and a flowchart in Fig. 2 provides a more comprehensive explanation of the technique. Utilizing the following substitutions

$$\begin{aligned}&[f,f',f'',\theta,\theta',\phi,\phi']=[y_1,y_2,y_3,y_4,y_5,y_6,y_7].\\&\text{where}\quad \frac{\partial y_1}{\partial\eta}=y_2,\quad \frac{\partial y_2}{\partial\eta}=y_3,\quad \frac{\partial y_4}{\partial\eta}=y_5,\quad \frac{\partial y_6}{\partial\eta}=y_7,\\&\qquad\qquad \frac{\partial y_3}{\partial\eta}=yy_1,\quad \frac{\partial y_5}{\partial\eta}=yy_2,\quad \frac{\partial y_7}{\partial\eta}=yy_3.\end{aligned} \tag{18}$$

$$yy_1=-\frac{1}{\gamma+\delta(y_3)^2}\left[y_1y_3-(y_2)^2+M(r-y_2)+r^2+\epsilon(y_4+Ry_6)\right], \tag{19}$$

$$yy_2=-\frac{1}{1+4Rd/3}\left[Pry_1y_5+PrNby_5y_7+PrNt(y_5)^2+MPrEc(y_2)^2\right], \tag{20}$$

$$\begin{aligned}yy_3=-\frac{Nt}{Nb}&\left(-\frac{1}{1+4Rd/3}\left[Pry_1y_5+PrNby_5y_7+PrNt(y_5)^2+MPrEc(y_2)^2\right]\right)\\&-LePry_1y_7+LePr\beta y_6.\end{aligned} \tag{21}$$

The initial conditions will be as follows:

$$\begin{aligned}&y_1=S,\quad y_2=1,\quad y_3=u_1,\quad y_4=1,\\&y_5=u_2,\quad y_6=1,\quad y_7=u_3\quad\text{at}\quad\eta=0.\end{aligned} \tag{22}$$

Table 1
Findings for skin friction w.r.t. physical parameters when $Ec = 2.0$, $Nb = Nt = 0.2$, $Le = 0.5$, $Pr = 6.8$, $\beta = 0.5$.

γ	δ	M	r	ϵ	R	C_f for assisting flow	C_f for opposing flow
0.2	0.2	0.1	1.0	0.1	0.5	0.0430	-0.0434
0.4						0.0493	-0.0496
0.6						0.0542	-0.0545
0.1	0.2					0.0414	-0.0421
	0.4					0.0454	-0.0461
	0.6					0.0485	-0.0494
		1.0				0.1735	-0.1540
		2.0				0.4573	-0.3084
		3.0				0.8115	-0.4569
			1.2			0.4706	0.2629
			1.4			1.1675	0.8964
			1.6			2.0814	1.7630
				0.2		0.1015	-0.1050
				0.4		0.2647	-0.2823
				0.6		0.4615	-0.5046
					1.0	0.6085	-0.0550
					1.5	0.7614	-0.0692
					2.0	0.9188	-0.0846

Above mentioned set of non-linear ordinary differential equations with initial conditions are resolved using Runge kutta with shooting method in MATLAB. The above mentioned initial conditions are u_1, u_2, u_3 which are attained by approximation using Newton's method until the following boundary conditions $y_2 \to r, \quad y_4 \to 0, \quad y_6 \to 0 \quad \text{at} \quad \eta \to \infty$ are obtained.

4. Numerical findings and discussion

Simulation and numerical techniques are performed over Eqs. (19) to (21) by using Eq. (22) for various physical parameters like Eyring-Prandtl fluid γ, elasticity δ, stagnation parameter r, Lewis number Le, thermal radiation parameter Rd, Eckert number Ec, chemical reaction parameter β etc. In both buoyancy regions, the values of the physical quantities like Skin friction coefficient, Nusselt number, and Sherwood number are computed for mass transfer, energy transfer, and flow, respectively. Table 1 shows the variation of skin friction coefficient against different parameters. For assisting flow value of C_f rises for Eyring-prandtl fluid parameter, elastic parameter, magnetic parameter, stagnation value, buoyancy temperature parameter and buoyancy ratio due to amplified fluid viscosity intensified buoyant forces and enhanced resistance to deformation, respectively, all contributing to increased frictional resistance along the surface, impeding fluid flow. While for opposing flow it only rises for stagnation parameter. Table 2 and 3 shows the behavior of Nusselt and Sherwood number in both regions. Energy transfer rate increases by the rise in the values of prandtl number for both buoyancy assisting and resisting flow and declines for remaining physical quantities. The mass transfer rate rises with the enhancement of thermal radiation value, prandtl number, thermophoresis, Eckert number, Lewis number, chemical reaction and magnetic parameter. For opposing flow mass transfer ratio only decreases for Brownian motion parameter. Graphical results of above mentioned parameters are observed across velocity f', temperature θ and nano particle concentration ϕ boundary layer. Comparison of present and existing study for reduced Nusselt number, Nusselt number and Sherwood number is made in Table 4, 5 and 6 respectively.

For velocity profile: Fig. 3 illustrates how the magnetic parameter affects the velocity gradient in the buoyancy-assisting and opposing flow region. Velocity profile exhibits different behavior for both regions. For assisting flow region the velocity increases because certain configurations of magnetic fields can induce instabilities in the flow, such as the magnetorotational instability (MRI) in accretion disks. These instabilities can lead to enhanced turbulence and increased velocity fluctuations, promoting overall higher velocities in the fluid. For the resisting flow velocity profile shows opposite behavior as value of M rises. A Lorentz force is created when a magnetic field and an electrically conductive fluid are combined. The force of the magnetic field opposing the transport phenomena causes the fluid's velocity within the boundary layer to decrease, preventing flow. Fig. 4 illustrates how the Eyring-Prandtl fluid parameter affects the velocity of the nanofluid in the flow areas that aid and resist buoyancy. When the Eyring-Prandtl fluid parameter rises in a buoyancy-assisting region, initially, the velocity profile tends to decrease due to enhanced thermal diffusion. This results in a more pronounced thermal boundary layer, slowing down the fluid near the boundary. However, as the Eyring-Prandtl parameter further increases, the thermal buoyancy effect becomes more dominant, leading to a stronger upward motion of fluid parcels in the boundary layer. Consequently, the velocity profile starts to rise as the buoyancy-driven flow becomes more significant, overcoming the damping effect of increased thermal diffusion near the boundary. In a buoyancy-opposing region, an increase in the Eyring-Prandtl fluid parameter initially accelerates fluid motion due to reduce coefficient of thermal diffusion, causing a thinner temperature boundary layer and faster velocity near the boundary. However, as the Eyring-Prandtl parameter further rises, the dominance of thermal buoyancy weakens, allowing thermal diffusion to play a more significant role. Consequently, the velocity profile begins to decrease

Table 2
Results for Nusselt number for assisting flow corresponding to physical parameters when $\gamma = 0.2, \delta = 0.2, \epsilon = 0.1, R = 0.5, r = 1.0, S = 0.5$.

Rd	Pr	Nb	Nt	Ec	Le	β	M	Nu_x for assisting flow	Nu_x for opposing flow
1.0	6.8	0.2	0.2	2.0	0.5	0.5	0.1	0.6324	0.6455
1.5								0.5934	0.6036
2.0								0.5606	0.5689
0.5	0.5							0.2983	0.2981
	1.0							0.3957	0.3975
	1.5							0.4639	0.4677
		1.0						0.0040	0.0054
		1.2						-0.0279	-0.0242
		1.4						-0.0392	-0.0365
			1.2					0.2120	0.2272
			1.4					0.1585	0.1740
			1.6					0.1130	0.1290
				2.0				0.6781	0.6956
				4.0				-0.4152	-0.3166
				6.0				-1.7989	-1.5290
					0.2			0.8060	0.8291
					0.4			0.7070	0.7257
					0.6			0.6561	0.6726
						0.2		0.6906	0.7089
						0.4		0.6820	0.6998
						0.6		0.6745	0.6917
							0.2	-0.4138	-0.3180
							0.4	-3.5302	-2.9991
							0.6	-8.4874	-6.8282

Table 3
Calculated values of Sherwood number for assisting flow with respect to physical parameters when $\gamma = 0.2, \delta = 0.2, \epsilon = 0.1, R = 0.5, r = 1.0, S = 0.5$.

Rd	Pr	Nb	Nt	Ec	Le	β	M	Sh_x for assisting flow	Sh_x for opposing flow
1.0	6.8	0.2	0.2	2.0	0.5	0.5	0.1	2.8953	2.8624
1.5								2.9161	2.8854
2.0								2.9334	2.9042
0.5	0.5							0.4973	0.4864
	1.0							0.7532	0.7374
	1.5							0.9720	0.9526
		1.0						3.1567	3.1358
		1.2						3.1468	3.1260
		1.4						3.1378	3.1169
			1.2					3.9755	3.8655
			1.4					4.3612	4.2375
			1.6					4.7542	4.6167
				2.0				2.8718	2.8353
				4.0				3.6077	3.5041
				6.0				4.5991	4.3589
					0.2			1.2621	1.2230
					0.4			2.3845	2.3473
					0.6			3.3329	3.2970
						0.2		2.5935	2.5514
						0.4		2.7824	2.7442
						0.6		2.9584	2.9234
							0.2	3.6062	3.5056
							0.4	5.9036	5.4542
							0.6	9.8868	8.4865

Table 4
Comparison of findings for reduced Nusselt number $-\theta'(0)$.

Pr	Khan Pop [56]	Wang [57]	Gorla and Sidawi [58]	Soomro et al. [54]	Current results
0.07	0.0663	0.0656	0.0656	0.0663	0.0688
0.20	0.1691	0.1691	0.1691	0.1691	0.1683
0.70	0.4539	0.4539	0.5349	0.4539	0.4545
2.00	0.9113	0.9114	0.9114	0.9113	0.9030
7.00	1.8954	1.8954	1.8905	1.8954	1.9031
20.00	3.3539	3.3539	3.3539	3.3539	3.3426
70.00	6.4621	6.4622	6.4622	6.4621	6.3509

Table 5
Comparison table of Nusselt number $-\theta'(0)$ with Nb and Nt taking $Pr = 10.0$ and $Le = 1.0$.

$Nb \rightarrow$ $Nt \downarrow$	0.1 Current	0.1 [56]	0.2 Current	0.2 [56]	0.3 Current	0.3 [56]	0.4 Current	0.4 [56]	0.5 Current	0.5 [56]
0.1	0.9383	0.9524	0.5054	0.5056	0.2519	0.2522	0.1193	0.1194	0.0542	0.0543
0.2	0.6844	0.6932	0.3776	0.3654	0.1817	0.1816	0.0818	0.0859	0.0359	0.0390
0.3	0.5206	0.5201	0.2515	0.2731	0.1467	0.1355	0.0689	0.0641	0.0208	0.0291
0.4	0.4099	0.4026	0.2270	0.2110	0.1002	0.1046	0.0498	0.0495	0.0224	0.0225
0.5	0.3232	0.3211	0.1041	0.1681	0.0871	0.0833	0.0340	0.0394	0.0178	0.0179

Table 6
Comparison of results of Sherwood number $-\phi'(0)$ with Nb and Nt taking $Pr = 10.0$ and $Le = 1.0$.

$Nb \rightarrow$ $Nt \downarrow$	0.1 Current	0.1 [56]	0.2 Current	0.2 [56]	0.3 Current	0.3 [56]	0.4 Current	0.4 [56]	0.5 Current	0.5 [56]
0.1	2.1607	2.1294	2.3195	2.3819	2.4258	2.4100	2.3701	2.3997	2.2906	2.3936
0.2	2.2128	2.2740	2.8051	2.5152	2.5177	2.5150	2.3823	2.4807	2.4255	2.4468
0.3	2.5015	2.5286	2.6052	2.6555	2.6373	2.6088	2.5398	2.5468	2.4783	2.4984
0.4	2.7073	2.7952	2.7207	2.7818	2.6798	2.6876	2.5799	2.6038	2.5200	2.5399
0.5	2.9126	3.0351	2.8743	2.8883	2.7412	2.7519	2.6302	2.6483	2.5563	2.5731

as the enhanced thermal diffusion dampens fluid motion near the boundary, resulting in a slower velocity gradient across the flow. Fig. 5 shows the effect of radiation parameter on velocity. Thermal radiation variations can have an impact on buoyant forces, which play an important role in fluid movement. The velocity increases for assisting flow and decreases for opposing flow as radiation parameter increases. In this scenario, the increased radiation parameter enhances radiative heating, leading to a stronger upward thermal gradient. This intensified buoyancy force accelerates fluid motion upwards, resulting in increased velocity. The additional thermal energy from radiation amplifies the buoyancy-driven flow, driving fluid parcels upwards at a faster rate. The enhanced radiative cooling effectively counteracts the buoyant forces, slowing down fluid motion and reducing the velocity gradient across the flow. Fig. 6 illustrates how elasticity affects the Eyring-Prandtl nanofluid flow velocity in the buoyancy-opposing and accommodating flow zones. Increased elasticity enhances the elasticity-induced stress, which acts against fluid motion. Consequently, in a buoyancy-assisting region, where buoyancy forces aid fluid motion, the increased elasticity opposes this motion, leading to a decrease in velocity. Conversely, in a buoyancy-opposing region, where buoyancy forces hinder fluid motion, the increased elasticity reinforces this opposition. The stronger elasticity-induced stress acts to resist the buoyancy-induced flow, leading to a rise in velocity.

For thermal profile: Fig. 7 shows the temperature increases for both layers. In a buoyancy-assisting and resisting zone, raising the radiation parameter can result in a larger contribution of radiative heat transfer. For buoyancy assisting region, the increased radiation parameter enhances radiative heating, leading to higher temperatures. Radiative heating adds thermal energy to the fluid, reinforcing the buoyancy-driven flow by creating a stronger upward thermal gradient. As a result, the temperature profile enhanced as more heat is absorbed by the fluid. In a buoyancy-resisting region, an increment in the radiation parameter leads to higher temperatures due to intensified radiative heating. As the radiation parameter increases, radiative heating becomes more dominant, adding thermal energy to the fluid. This results in a stronger upward thermal gradient, even in regions where buoyancy forces oppose fluid motion. The temperature profile increases with an increase in the thermophoresis parameter shown in Fig. 8. An increase in thermophoresis parameter may result in improved particle migration towards regions of higher or lower temperature, depending on the characteristics of the particles, in a both buoyancy zones. The random motion of suspended particles intensifies the temperature within the fluid as shown in Fig. 9. Increases in the Brownian motion parameter can cause more intense and erratic particle movement in a buoyancy-assisting zone where temperature gradients cooperate the flow. Hence the temperature of flow rises. Similarly, in a buoyancy-resisting region, the heightened Brownian motion promotes better mixing and heat transfer despite the opposition from buoyancy forces. The increased Brownian motion facilitates the dispersal of thermal energy, leading to higher temperatures throughout the region.

For concentration profile: Radiation parameter has a significant effect on the mass concentration of fluid flow in Fig. 10. For $\eta < 0.7$ the concentration profile decreases for both assisting and opposing areas and vice versa with the increment in radiation parameter. The reason is that Initially, with lower values of η, the increase in the radiation parameter intensifies radiative heating, leading to

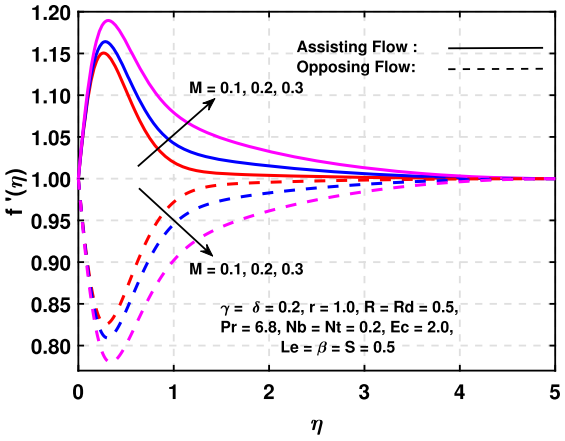

Fig. 3. Impact of magnetic field on velocity.

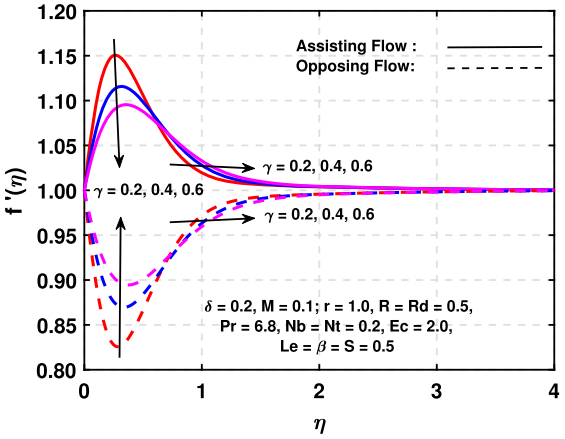

Fig. 4. Impact of prandtl fluid parameter on velocity.

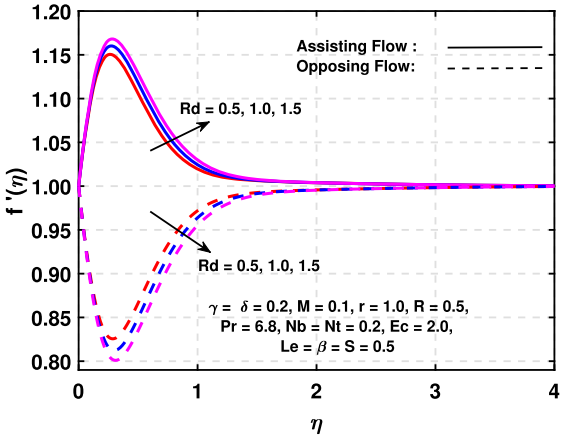

Fig. 5. Impact of radiation parameter on velocity.

higher temperatures in the fluid. Consequently, the concentration of the substance decreases in this region as the substance is transported away more rapidly due to enhanced thermal effects. The concentration of the substance starts to increase beyond $\eta < 0.7$ as the convective mixing overcomes the initial mass transfer away from the boundary, leading to a rise in the concentration profile. Here $\eta = 0.7$ is considered because curves shows distinct behavior at this stage. Fig. 11 shows that the concentration profile increases for both buoyancy layers with rise in thermophoretic effect. When the thermophoresis parameter increases, particles migrate more efficiently towards regions of higher temperature, leading to increased accumulation near the boundary in both buoyancy-assisting

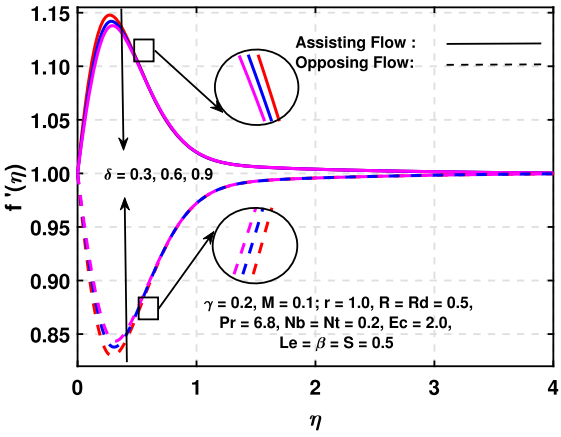

Fig. 6. Impact of elastic parameter on velocity.

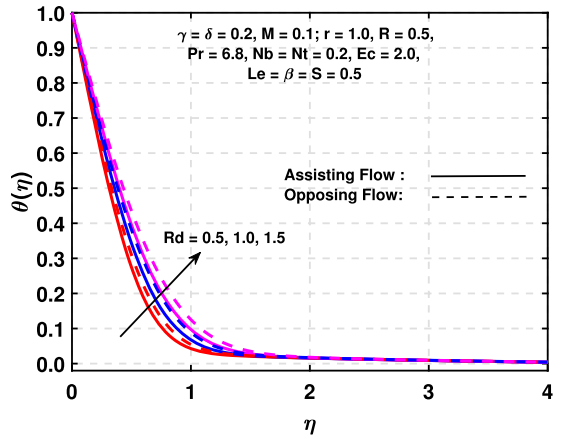

Fig. 7. Impact of radiation on thermal profile.

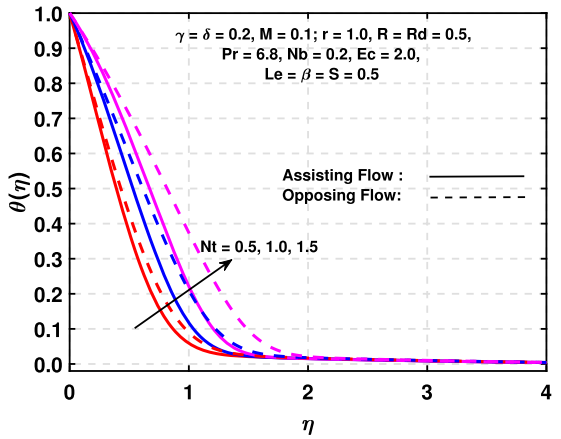

Fig. 8. Impact of thermophoresis parameter on thermal profile.

and resisting regions, consequently raising the concentration profile due to enhanced thermophoretic effects. Fig. 12 displays that the profile of mass transfer decreases with the increment of Brownian motion parameter. When the Brownian motion parameter increases, particles exhibit more random motion, causing enhanced dispersion away from the boundary in both buoyancy-assisting and resisting regions, thus decreasing the concentration profile due to increased particle dispersion. The mass transfer ratio decreases by rising Lewis number in Fig. 13. Mass transfer rates reduces which is results from the substance's difficulty diffusing through the fluid when Le rises. Fig. 14 shows the impact of chemical reaction parameter on mass transfer profile. Mass transfer in a fluid flow

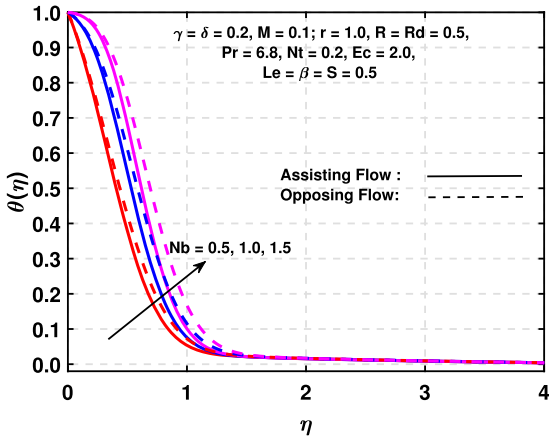

Fig. 9. Impact of Brownian motion parameters on thermal profile.

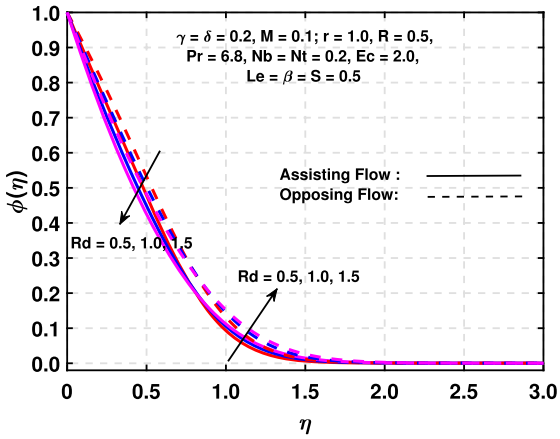

Fig. 10. Impact of radiation parameters on concentration.

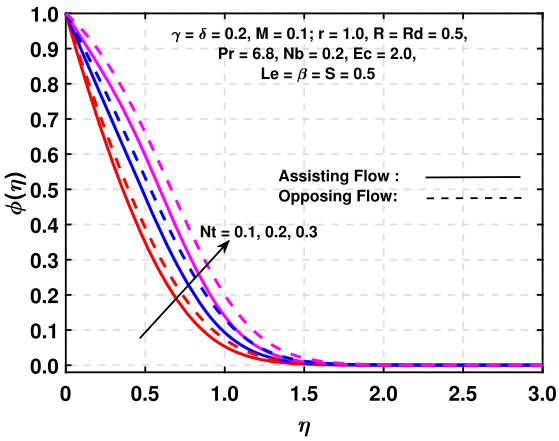

Fig. 11. Impact of thermophoresis parameter on concentration.

can be improved by raising the chemical reaction rate. This is mainly due to the fact that chemical interactions in different ways make it easier for substances to move between various phases, such as between two liquids or between a gas and a liquid.

The Fig. 15(a)-15(b) and Fig. 15(c)-15(d) are drawn to study the flow pattern for rising values of magnetic field and radiation parameter in case of both aiding and opposing flows, respectively. From these figures it is revealed that streamlines are congested and more symmetrical for aiding flow where for opposing flow streamlines are more distanced. Furthermore, an increase in magnetic parameter

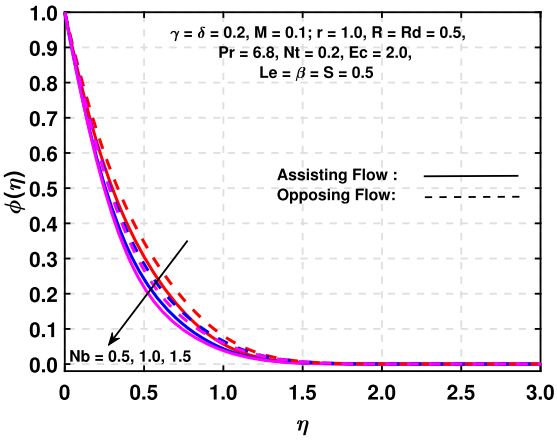

Fig. 12. Impact of Brownian motion parameters on concentration.

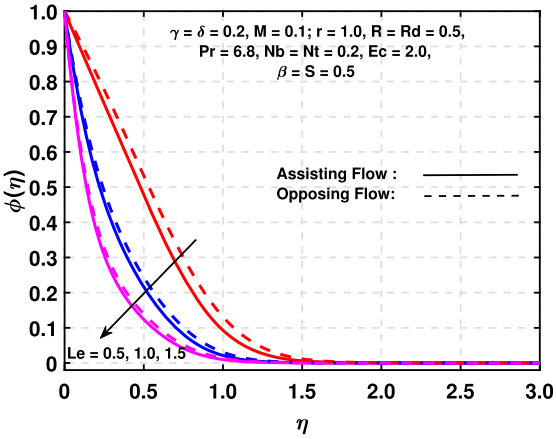

Fig. 13. Impact of Lewis number on concentration.

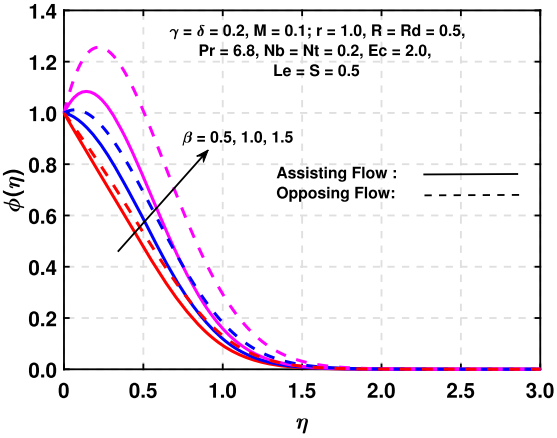

Fig. 14. Impact of chemical reaction parameter on concentration.

and radiation parameter squeezes the streamlines significantly in presence of assisting flow while opposite trend is witnessed in case of opposing flow respectively.

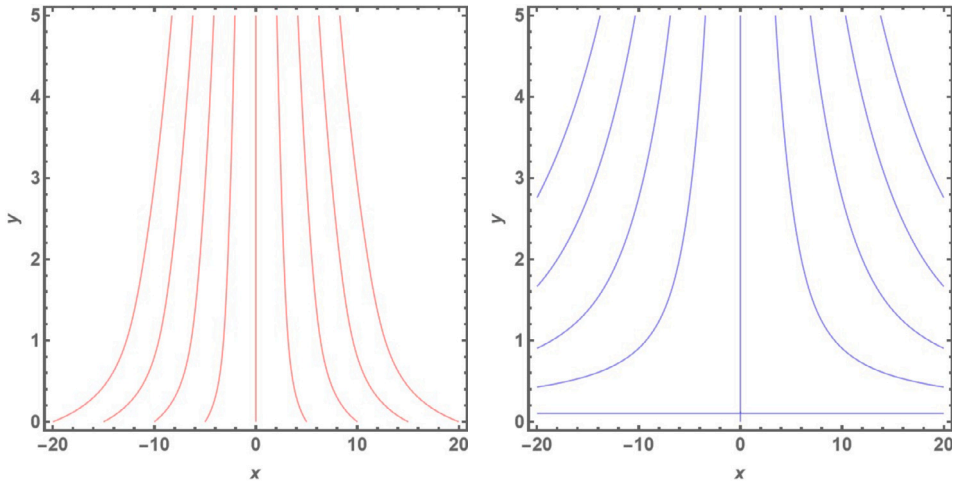

(a) For assisting flow. (b) For opposing flow.

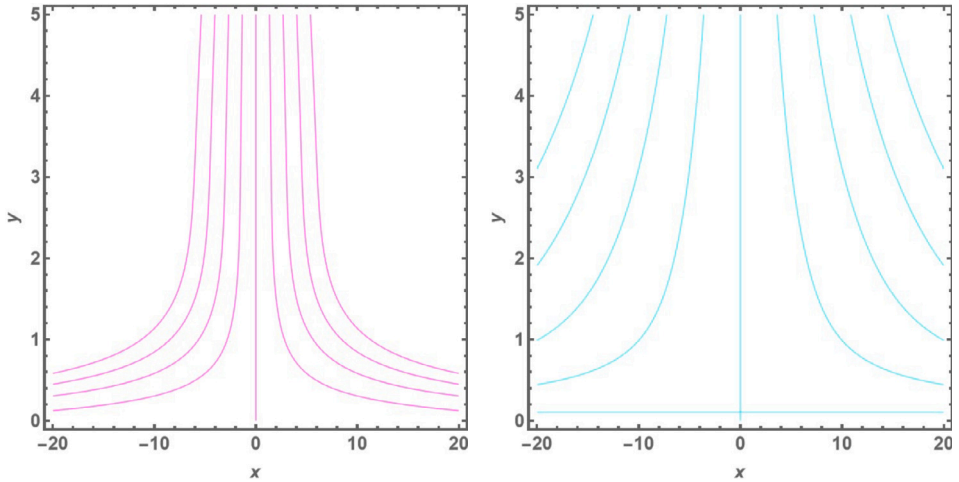

(c) For assisting flow. (d) For opposing flow.

Fig. 15. Streamlines for various values of magnetic parameter.

5. Concluding remarks

This study investigates heat transfer effects on Eyring-Prandtl fluid, previously unstudied, providing a foundation for future research. Focusing on non-Newtonian nanofluids, it analyzes thermophoretic and Brownian motion effects on a stretching sheet under a vertical magnetic field. Incorporating Joule heating, thermal radiation, and chemical reactions, it explores the potential applications of Eyring-Prandtl fluid in enhancing energy and mass transfer processes. By utilizing similarity transformations and numerical methods like the Runge Kutta method with bvp4c in MATLAB, the study effectively tackles the system of partial differential equations. A comprehensive examination gives some important results, summarized as follows:

- The Eyring-Prandtl fluid factor, buoyancy ratios, and stagnation effect all had a beneficial influence on the fluid's skin friction in the flow-assisting zone in ascending order. While for opposing region this led to converse behavior.
- The magnetic field parameter enhances the heat conductance of the fluid flow that give rise to flow rate at the surface as well as in the boundary layers.
- The velocity profile begins to ascend as the buoyancy-driven flow gains prominence, surpassing the damping influence of heightened thermal diffusion near the boundary.
- Increases in the Brownian motion parameter can cause more intense and erratic particle movement in a buoyancy-assisting zone where temperature gradients cooperate the flow. Hence the temperature of flow rises.
- Mass transfer rate is positively affected by rising values of radiation factor, Prandtl number, thermophoretic impact and Lewis number in buoyancy assisting region.

- As the thermophoresis parameter rises, particles exhibit enhanced migration towards areas of elevated temperature, resulting in heightened accumulation near the boundary in both buoyancy-assisting and buoyancy-resisting regions.

Limitations:

- The results are valid only for aiding and resisting flow.
- The obtained results are authenticated for specific fluid i-e Eyring-Prandtl fluid.

The most prominent result of the present investigation includes the fact that presence of nanofluid highly influence the assisting and opposing fluid flow phenomenon. The findings of the current study on heat and mass transfer through a stretching sheet, considering the effects of thermophoresis, Brownian motion, and chemical reactions, can significantly influence engineering applications such as advanced material development, environmental and biomedical engineering, industrial process optimization, and the design of enhanced heat exchanger systems. Keeping in view the prominent application of presented set up in various engineering applications, authors aim to extend this investigation by exploring thermal convection effects at the surface. In the realm of investigating the behavior of Eyring-Prandtl fluids subjected to Joule heating and Brownian motion, future endeavors could focus on refining computational models to capture the intricate interplay between these phenomena with higher accuracy and resolution. Investigating the influence of surface interactions, such as boundary conditions and surface roughness, could unveil additional complexities and phenomena crucial for practical applications.

CRediT authorship contribution statement

E.N. Maraj: Writing – review & editing, Software, Conceptualization. **Harsa Afaq:** Writing – original draft. **Ehtsham Azhar:** Supervision. **Muhammad Jamal:** Visualization. **Haitham A. Mahmoud:** Data curation.

Declaration of competing interest

The authors declare the following financial interests/personal relationships which may be considered as potential competing interests: Haitham A. Mahmoud reports financial support was provided by Industrial Engineering Department, College of Engineering, King Saud University, Riyadh 11421, Saudi Arabia. If there are other authors, they declare that they have no known competing financial interests or personal relationships that could have appeared to influence the work reported in this paper.

Data availability

No data was used for the research described in the article.

Acknowledgements

The authors present their appreciation to King Saud University for funding this research through Researchers Supporting Program number (RSPD2024R1006), King Saud University, Riyadh, Saudi Arabia.

References

[1] Stephen U.S. Choi, J.A. Eastman, Enhancing thermal conductivity of fluids with nanoparticles, 1995.
[2] M.A. El-Shorbagy, Farshad Eslami, Muhammad Ibrahim, Pouya Barnoon, Wei-Feng Xia, Davood Toghraie, Numerical investigation of mixed convection of nanofluid flow in a trapezoidal channel with different aspect ratios in the presence of porous medium, Case Stud. Therm. Eng. 25 (2021) 100977.
[3] Yeping Peng, Milad Boroumand Ghahnaviyeh, Mohammad Nazir Ahmad, Ali Abdollahi, Seyed Amin Bagherzadeh, Hamidreza Azimy, Amirhosein Mosavi, Aliakbar Karimipour, Analysis of the effect of roughness and concentration of Fe3O4/water nanofluid on the boiling heat transfer using the artificial neural network: an experimental and numerical study, Int. J. Therm. Sci. 163 (2021) 106863.
[4] Yanjun Chen, Pingshan Luo, Deqiang He, Rui Ma, Numerical simulation and analysis of natural convective flow and heat transfer of nanofluid under electric field, Int. Commun. Heat Mass Transf. 120 (2021) 105053.
[5] M. Israr Ur Rehman, Haibo Chen, Aamir Hamid, Wasim Jamshed, Mohamed R. Eid, Sayed M. El Din, Hamiden Abd El-Wahed Khalifa, Assmaa Abd-Elmonem, Effect of Cattaneo-Christov heat flux case on Darcy-Forchheimer flowing of sutterby nanofluid with chemical reactive and thermal radiative impacts, Case Stud. Therm. Eng. 42 (2023) 102737.
[6] M. Israr Ur Rehman, Haibo Chen, Aamir Hamid, Sajid Qayyum, Wasim Jamshed, Zehba Raizah, Mohamed R. Eid, El Sayed M. Tag El Din, Soret and Dufour influences on forced convection of cross radiative nanofluid flowing via a thin movable needle, Sci. Rep. 12 (1) (2022) 18666.
[7] Jiayou Du, Ruijin Wang, Qiuyi Zhuo, Weijia Yuan, Heat transfer enhancement of Fe3O4-water nanofluid by the thermo-magnetic convection and thermophorestic effect, Int. J. Energy Res. 46 (7) (2022) 9521–9532.
[8] Yanwei Hu, Yurong He, Shufu Wang, Qizhi Wang, H. Inaki Schlaberg, Experimental and numerical investigation on natural convection heat transfer of tio2–water nanofluids in a square enclosure, J. Heat Transf. 136 (2) (2014) 022502.
[9] Ean Hin Ooi, Viktor Popov, Numerical study of influence of nanoparticle shape on the natural convection in cu-water nanofluid, Int. J. Therm. Sci. 65 (2013) 178–188.
[10] Jincheng Zhou, Masood Ashraf Ali, As' ad Alizadeh, Sattam Fahad Almojil, Pradeep Kumar Singh, Abdulaziz Ibrahim Almohana, Abdulrhman Fahmi Alali, Numerical investigation, environmental consideration, and the use of machine learning in optimizing the dimensions of a rectangular blade between two blades in the presence of a magnetic field (two-phase method), Eng. Anal. Bound. Elem. 149 (2023) 71–85.

[11] M. Israr Ur Rehman, Haibo Chen, Wasim Jamshed, Mohamed R. Eid, Kamel Guedri, Sayed M. El Din, Thermal radiative flux and energy of Arrhenius evaluation on stagnating point flowing of Carreau nanofluid: a thermal case study, Case Stud. Therm. Eng. 40 (2022) 102583.
[12] Xianqin Zhang, Dezhi Yang, M. Israr Ur Rehman, A.A. Mousa, Aamir Hamid, Numerical simulation of bioconvection radiative flow of Williamson nanofluid past a vertical stretching cylinder with activation energy and swimming microorganisms, Case Stud. Therm. Eng. 33 (2022) 101977.
[13] Junfeng Yin, Xianqin Zhang, M. Israr Ur Rehman, Aamir Hamid, Thermal radiation aspect of bioconvection flow of magnetized sisko nanofluid along a stretching cylinder with swimming microorganisms, Case Stud. Therm. Eng. 30 (2022) 101771.
[14] Aamir Hamid, Masood Khan, Abdul Hafeez, et al., Unsteady stagnation-point flow of Williamson fluid generated by stretching/shrinking sheet with ohmic heating, Int. J. Heat Mass Transf. 126 (2018) 933–940.
[15] Aamir Hamid, Masood Khan, et al., Impacts of binary chemical reaction with activation energy on unsteady flow of magneto-Williamson nanofluid, J. Mol. Liq. 262 (2018) 435–442.
[16] Masood Khan, Aamir Hamid, et al., Numerical investigation on time-dependent flow of Williamson nanofluid along with heat and mass transfer characteristics past a wedge geometry, Int. J. Heat Mass Transf. 118 (2018) 480–491.
[17] Harsa Afaq, Ehtsham Azhar, Muhammad Jamal, Hashmat Ali, Influence of magnetohydrodynamics on Casson nanofluid heat transfer over a radiating stretching surface, Int. J. Comput. Mater. Sci. Eng. (2024) 2450003.
[18] Mohamed R. Eid, K.L. Mahny, Ahmed F. Al-Hossainy, Homogeneous-heterogeneous catalysis on electromagnetic radiative Prandtl fluid flow: Darcy-Forchheimer substance scheme, Surf. Interfaces 24 (2021) 101119.
[19] Amar B. Patil, Pooja P. Humane, Vishwambhar S. Patil, Govind R. Rajput, Mhd Prandtl nanofluid flow due to convectively heated stretching sheet below the control of chemical reaction with thermal radiation, Int. J. Ambient Energy 43 (1) (2022) 4310–4322.
[20] A. Abbasi, F. Mabood, W. Farooq, S.U. Khan, Radiation and Joule heating effects on electroosmosis-modulated peristaltic flow of Prandtl nanofluid via tapered channel, Int. Commun. Heat Mass Transf. 123 (2021) 105183.
[21] M.D. Shamshuddin, Zehba Raizah, Nevzat Akkurt, Vishwambhar S. Patil, Sayed M. Eldin, Case study of thermal and solutal aspects on non-Newtonian Prandtl hybrid nanofluid flowing via stretchable sheet: multiple slip solution, Case Stud. Therm. Eng. 49 (2023) 103186.
[22] Amar B. Patil, Vishwambhar S. Patil, Pooja P. Humane, M.D. Shamshuddin, Govind R. Rajput, Mhd-driven chemically active and thermally radiative Prandtl hybrid nanofluid flow on stretching device with ohmic heating, dissipation, and diffusion effects, Numer. Heat Transf., Part A, Appl. (2023) 1–18.
[23] Rahmat Ellahi, Arshad Riaz, S. Nadeem, A theoretical study of Prandtl nanofluid in a rectangular duct through peristaltic transport, Appl. Nanosci. 4 (2014) 753–760.
[24] Muhammad Hamid, Tamour Zubair, Muhammad Usman, Zafar Hayat Khan, Wei Wang, Natural convection effects on heat and mass transfer of slip flow of time-dependent Prandtl fluid, J. Comput. Des. Eng. 6 (4) (2019) 584–592.
[25] Othmane Oulaid, Brahim Benhamou, Nicolas Galanis, Simultaneous heat and mass transfer in inclined channel with asymmetrical conditions, in: International Heat Transfer Conference, vol. 49378, 2010, pp. 351–359.
[26] Khilap Singh, Alok Kumar Pandey, Manoj Kumar, Entropy generation impact on flow of micropolar fluid via an inclined channel with non-uniform heat source and variable fluid properties, Int. J. Appl. Comput. Math. 6 (2020) 1–12.
[27] Torikul Islam, M. Ferdows, M.D. Shamshuddin, Marei Saeed Alqarni, Usman, Sisko fluid modeling and numerical convective heat transport analysis over-stretching device with radiation and heat dissipation, Numer. Heat Transf., Part A, Appl. 85 (8) (2024) 1240–1258.
[28] M.D. Shamshuddin, Anwar Saeed, S.R. Mishra, Ramesh Katta, Mohamed R. Eid, Homotopic simulation of mhd bioconvective flow of water-based hybrid nanofluid over a thermal convective exponential stretching surface, Int. J. Numer. Methods Heat Fluid Flow 34 (1) (2024) 31–53.
[29] M.D. Shamshuddin, S.O. Salawu, K. Ramesh, Vishwambhar S. Patil, Pooja Humane, Bioconvective treatment for the reactive Casson hybrid nanofluid flow past an exponentially stretching sheet with ohmic heating and mixed convection, J. Therm. Anal. Calorim. 148 (21) (2023) 12083–12095.
[30] Yijie Li Usman, M.D. Shamshuddin, Govind R. Rajput, A. Ghaffari, Taseer Muhammad, Exploration of nonlinear radiative heat energy on Buongiorno modeled nano liquid toward an inclined porous plate with heat source and variable chemical reaction, Numer. Heat Transf., Part A, Appl. (2023) 1–20.
[31] Irfan Mustafa, Abuzar Ghaffari, M. Saleem Iqbal, et al., Unsteady heat and mass transfer in a stagnant flow towards a stretching porous sheet with variable fluid properties, in: Mathematical Modelling of Fluid Dynamics and Nanofluids, CRC Press, 2024, pp. 117–137.
[32] Zhihong He, Muhammad Bilal Arain, W.A. Khan, Ali Rashash R. Alzahrani, Taseer Muhammad, A.S. Hendy, Mohamed R. Ali, et al., Theoretical exploration of heat transport in a stagnant power-law fluid flow over a stretching spinning porous disk filled with homogeneous-heterogeneous chemical reactions, Case Stud. Therm. Eng. 50 (2023) 103406.
[33] Farwa Asmat, W.A. Khan, Ilyas Khan, Taseer Muhammad, et al., A scientific report on Stokes' second problem for a transient nanofluid model with a heated boundary in the presence of a magnetic field, J. Magn. Magn. Mater. 586 (2023) 171171.
[34] Uddhaba Biswal, Snehashish Chakraverty, Bata Krushna Ojha, Ahmed Kadhim Hussein, Numerical simulation of magnetohydrodynamics nanofluid flow in a semi-porous channel with a new approach in the least square method, Int. Commun. Heat Mass Transf. 121 (2021) 105085.
[35] Gomathy Govindasamy, Rushi Kumar Bangalore, Heat and mass transfer in thin film flow of Casson nanofluid over an unsteady stretching sheet, Proc. Inst. Mech. Eng., E J. Process Mech. Eng. (2023) 09544089221150727.
[36] G. Gomathy, B. Rushi Kumar, Thin film flow dynamics and heat transfer enhancement in porous media: shape-dependent behavior of al 2 o 3 nanoparticles, Numer. Heat Transf., Part A, Appl. (2024) 1–18.
[37] G. Gomathy, B. Rushi Kumar, Impacts of nanoparticle shapes on ag-water nanofluid thin film flow through a porous medium with thermal radiation and ohmic heating, J. Therm. Anal. Calorim. (2023) 1–19.
[38] A.S. Sabu, Alphonsa Mathew, T.S. Neethu, K. Anil George, Statistical analysis of mhd convective ferro-nanofluid flow through an inclined channel with Hall current, heat source and Soret effect, Therm. Sci. Eng. Prog. 22 (2021) 100816.
[39] Muhammad Jawad, Anwar Saeed, Muhammad Bilal, Taza Gul, Arshad Khan, Saleem Nasir, The impact of magnetohydrodynamic on bioconvection nanofluid flow with viscous dissipation and Joule heating effects, Eng. Res. Express 3 (1) (2021) 015030.
[40] Syed Asif Ali Shah, N. Ameer Ahammad, Bagh Ali, Kamel Guedri, Aziz Ullah Awan, Fehmi Gamaoun, ElSayed M. Tag-ElDin, Significance of bio-convection, mhd, thermal radiation and activation energy across Prandtl nanofluid flow: a case of stretching cylinder, Int. Commun. Heat Mass Transf. 137 (2022) 106299.
[41] Imad Khan, Arif Hussain, M.Y. Malik, Safyan Mukhtar, On magnetohydrodynamics Prandtl fluid flow in the presence of stratification and heat generation, Phys. A, Stat. Mech. Appl. 540 (2020) 123008.
[42] Kai-Long Hsiao, Micropolar nanofluid flow with mhd and viscous dissipation effects towards a stretching sheet with multimedia feature, Int. J. Heat Mass Transf. 112 (2017) 983–990.
[43] B.C. Prasannakumara, M.R. Krishnamurthy, B.J. Gireesha, Rama SR Gorla, Effect of multiple slips and thermal radiation on mhd flow of Jeffery nanofluid with heat transfer, J. Nanofluids 5 (1) (2016) 82–93.
[44] C.M. Mohana, B. Rushi Kumar, Nanoparticle shape effects on hydromagnetic flow of Cu-water nanofluid over a nonlinear stretching sheet in a porous medium with heat source, thermal radiation, and Joule heating, Z. Angew. Math. Mech. 104 (1) (2024) e202300188.
[45] C. Sowmiya, B. Rushi Kumar, Mathematical modeling of viscoelastic fluid flow across a nonlinear stretching surface in porous media with varying magnetic field, Int. J. Mod. Phys. B (2023) 2450348.
[46] Sravan Kumar, B. Rushi Kumar, Oluwole Daniel Makinde, A.G. Vijaya Kumar, Magneto-convective heat transfer in micropolar nanofluid over a stretching sheet with non-uniform heat source/sink, Defect and Diffusion Forum, vol. 387, Trans Tech Publ, 2018, pp. 78–90.
[47] V. Ramachandra Prasad, S. Abdul Gaffar, B. Rushi Kumar, Non-similar comutational solutions for double-diffusive mhd transport phenomena for non-newtnian nanofluid from a horizontal circular cylinder, Nonlinear Eng. 8 (1) (2019) 470–485.

[48] M. Sathish Kumar, N. Sandeep, B. Rushi Kumar, P.A. Dinesh, A comparative analysis of magnetohydrodynamic non-Newtonian fluids flow over an exponential stretched sheet, Alex. Eng. J. 57 (3) (2018) 2093–2100.
[49] N. Sandeep, M. Kumar, B. Kumar, J. Prakash, Effect of Cattaneo-Christov heat flux on nonlinear radiative mhd flow of Casson fluid induced by a semi-infinite stretching surface, Front. Heat Mass Transf. 8 (2017).
[50] A. Sumithra, R. Sivaraj, V. Ramachandra Prasad, O. Anwar Bég, Ho-Hon Leung, Firuz Kamalov, S. Kuharat, B. Rushi Kumar, Computation of inclined magnetic field, thermophoresis and Brownian motion effects on mixed convective electroconductive nanofluid flow in a rectangular porous enclosure with adiabatic walls and hot slits, Int. J. Mod. Phys. B (2023) 2450398.
[51] Ayman A. Gadelhak, Kh S. Mekheimer, M.A. Seddeek, R.E. Abo-Elkhair, Khalid K. Ali, Ahmed M. Salem, Energy transport of Williamson nano-fluid over a curved stretching surface by means of fdm, BioNanoScience 13 (3) (2023) 1116–1125.
[52] A.Z. Zaher, Khalid K. Ali, Kh S. Mekheimer, Electroosmosis forces eof driven boundary layer flow for a non-Newtonian fluid with planktonic microorganism: Darcy Forchheimer model, Int. J. Numer. Methods Heat Fluid Flow 31 (8) (2021) 2534–2559.
[53] Kh S. Mekheimer, Shaimaa F. Ramadan, New insight into gyrotactic microorganisms for bio-thermal convection of Prandtl nanofluid over a stretching/shrinking permeable sheet, SN Appl. Sci. 2 (3) (2020) 450.
[54] Feroz Ahmed Soomro, Rizwan Ul Haq, Muhammad Hamid, Brownian motion and thermophoretic effects on non-Newtonian nanofluid flow via Crank–Nicolson scheme, Arch. Appl. Mech. 91 (2021) 3303–3313.
[55] Wasim Jamshed, Marjan Goodarzi, M. Prakash, Kottakkaran Sooppy Nisar, M. Zakarya, Abdel-Haleem Abdel-Aty, et al., Evaluating the unsteady Casson nanofluid over a stretching sheet with solar thermal radiation: an optimal case study, Case Stud. Therm. Eng. 26 (2021) 101160.
[56] W.A. Khan, I. Pop, Boundary-layer flow of a nanofluid past a stretching sheet, Int. J. Heat Mass Transf. 53 (11–12) (2010) 2477–2483.
[57] C.Y. Wang, Free convection on a vertical stretching surface, Z. Angew. Math. Mech. 69 (11) (1989) 418–420.
[58] Rama Subba Reddy Gorla, Ibrahim Sidawi, Free convection on a vertical stretching surface with suction and blowing, Appl. Sci. Res. 52 (1994) 247–257.